Environmental Science and Pollution Research (2019) 26:21463–21474
https://doi.org/10.1007/s11356-019-05441-2

RESEARCH ARTICLE

Effects of fulvic acid on aggregation, sedimentation, and adsorption of Fe_3O_4 magnetic nanoparticles

Tianhui Zhao[1,2] · Mengyuan Fang[2,3] · Zhi Tang[2] · Xiaoli Zhao[2] · Fazhi Xie[4] · Fengchang Wu[2] · John P. Giesy[5,6]

Received: 14 March 2019 / Accepted: 9 May 2019 / Published online: 24 May 2019

Abstract

Environmental behavior, bioavailability, and risks posed by Fe_3O_4, magnetic nanoparticles (Fe_3O_4 NPs) in surface waters are affected by complex geochemistry, including pH and inorganic and organic matter. This work provides a systematic analysis of adsorption of fulvic acid (FA) on surfaces of Fe_3O_4 NPs with adsorption kinetics, adsorption thermodynamic, and adsorption isotherm. Adsorption of FA on surfaces of Fe_3O_4 NPs is consistent with assumptions of Langmuir and Freundlich adsorption isotherm models. The adsorption amount of FA was inversely proportional to solution pH, and the maximum amount is 128.6 mg g^{-1}. Adsorption of FA on surfaces of Fe_3O_4 NPs is a spontaneous endothermic process. FA plays an important role in aggregation and suspension/sedimentation behavior of Fe_3O_4 NPs in aquatic environmental. With continuous adsorption of FA, electrostatic repulsion between the particles and the steric hindrance of FA significantly decreased aggregation and increased suspension of Fe_3O_4 NPs. The results of FTIR and XPS indicated that FA was adsorbed on Fe_3O_4 NPs mainly through chemical reactions, and carbohydrates particularly play an important role in adsorption.

Keywords Aggregation · Adsorption thermodynamics · Adsorption kinetics · Suspension performance · Natural organic matter

Introduction

Due to their exceptional physicochemical properties, nanomaterials have been used widely for emerging applications, such as bioimaging, drug delivery, magnetics, electronics biomedicine, and catalysis. Among them, ferroferric oxide nanoparticles (Fe_3O_4 NPs) are useful for magnetic data storage, magnetic liquids, biomedicine, catalysis, and groundwater remediation due to the ease of separating them from aqueous media and reusability (Hassani et al. 2018a, b; Hu et al. 2005). This increasing application has resulted in greater discharge of Fe_3O_4 NPs into the environment during production, utilization, and disposal. Some studies have shown that Fe_3O_4 NPs can be toxic to *Brachionus rotundiformis* and algae (Mashjoor et al. 2018; Barhoumi and Dewez 2013). During long-time exposure of rats to Fe_3O_4 NPs, it has caused increased numbers of alveolar macrophages and neutrophil leucocytes in bronchoalveolar lavage fluid (Katsnelson et al. 2011). Also, Fe_3O_4 NPs might adsorb pollutants and interact with other nanoparticles to alter their bioavailability and accumulation into organisms and thus modulate toxicity. Once they enter aqueous environments, Fe_3O_4 NPs can undergo

Responsible editor: Tito Roberto Cadaval Jr

✉ Zhi Tang
tzwork@hotmail.com

✉ Xiaoli Zhao
zhaoxiaoli_zxl@126.com

[1] College of Water Sciences, Beijing Normal University, Beijing 100875, China

[2] State Key Laboratory of Environmental Criteria and Risk Assessment, Chinese Research Academy of Environmental Sciences, Beijing 100012, China

[3] Faculty of Environmental Science and Engineering, Kuming University of Science and Technology, Kuming 650550, Yunnan, China

[4] School of Material Science and Chemical Engineering, Anhui Jianzhu University, Hefei 230601, Anhui, China

[5] Department of Veterinary Biomedical Sciences and Toxicology Centre, University of Saskatchewan, Saskatoon, Saskatchewan, Canada

[6] Department of Environmental Science, Baylor University, Waco, TX, USA

complicated migration/conversion process and might cause significant adverse effects on ecosystems. Migration, transport, and fate of Fe_3O_4 NPs in aqueous environments are affected by local geochemistry, including pH, ionic strength, and natural organic matter (NOM) (Erhayem and Sohn 2014a; Erhayem and Sohn 2014b). Thus, to protect the health of ecosystems, investigating how the physical and chemical parameters of water affect environmental behaviors of Fe_3O_4 NPs was deemed appropriate.

Natural organic matter (NOM) is widely distributed in aqueous environment, which comprises a heterogeneous mixture of components. Fulvic acid (FA) is the major component of NOM and differs from humic acids (HA) in terms of its molecular masses, chemical composition, and functional groups, which can influence the suspension/sedimentation and ecological effects of Fe_3O_4 NPs. FA molecules, derived from plant materials, are a more recalcitrant fraction of NOM that has a large specific surface area with high surface energy, which contains a variety of reactive groups such as carboxylic acid, phenolic hydroxyl, hydroxyl groups, quinone, and amine. Due to deprotonation of these reactive groups, FA molecules can be adsorbed by hydrogen bonding, ion pairing, or chelate metal ions, forming transition metal complexes, which can modulate their bioavailability and toxic potencies. FA can be adsorbed by kaolinite (Li et al. 2008), silicon dioxide (Liang et al. 2011), α-Fe_2O_3 (He et al. 2017), and other nanomaterials (Baalousha 2009; Wei and Xiang 2013) and used to removal various pollutions in the water environment. Among those applications, the FA-coated Fe_3O_4 is widely used by its special physical and chemical properties. On the one hand, Fe_3O_4 NPs have the unique property that they can easily be separated from water by use of a magnetic field due to their superparamagnetic properties (Tang et al. 2016). On the other hand, FA can not only promote the suspension of Fe_3O_4 NPs but also have significant reactivities with other contaminants through various types of functional group such as carboxylate, phenolic, and carbonyl functional groups (Parfitt et al. 2006; Chappell et al. 2009; Pan and Xing 2008). The application of FA-coated Fe_3O_4 has obvious advantages, but its environmental behavior cannot be ignored. Toxicological studies have demonstrated that toxicity of nanomaterials (NMs) largely depends on their size and aggregation (Limbach et al. 2005; Panessa-Warren et al. 2009). Moreover, as an important factor, pH directly influences surface properties as well as charge density of NMs, which subsequently can affect interactions between NMs and organic compounds including FA. The degree of ionization, solubility, hydrophilicity, and crimp degree of NOM will also be affected (Hyung and Kim 2008; Lin et al. 2009). FA and pH ultimately control aggregation of NMs in suspension, as well as their attachment to environmental surfaces.

Results of previous studies have shown that HA can be absorbed and deposited on surfaces of Fe_3O_4 NPs, thereby affecting aggregation, suspension/sedimentation behaviors of Fe_3O_4 NPs, and other organic pollutants (Baalousha et al. 2009; Illés and Tombácz 2006; Pan and Xing 2008; Weng et al. 2006). However, few reports on effects of FA also are an important component of NOM on environmental behavior of Fe_3O_4 NPs in aqueous environments. Therefore, the result of this study will provide a system of understanding adsorption of FA on Fe_3O_4 NPs under various pHs and subsequently the suspension/sedimentation behavior of Fe_3O_4 NPs/FA complexes after adsorption, providing theoretical foundation for the investigation of environmental behavior and potential ecological effects of Fe_3O_4 NPs in aquatic environments.

Materials and methods

Materials

The chemicals including $FeCl_2$ $4H_2O$, $FeCl_3$ $6H_2O$, NaCl, HCl, and NaOH were obtained from Sinopharm Chemical Reagent Beijing Co., Ltd., China. All the chemicals used in the experiments were analytical reagent grade if not specified and were used without further purification.

Fe_3O_4 NPs were prepared by co-precipitation. A total of 2.0 g $FeCl_2 \cdot 4H_2O$ and 5.2 g $FeCl_3 \cdot 6H_2O$ were dissolved in 25 mL of deionized water, which had been pre-deoxidized by nitrogen. The solution was added dropwise into a 250-mL NaOH solution (1.5 M) under mechanical stirring and nitrogen flow. Black Fe_3O_4 NPs formed in the synthesis reaction were rinsed five times with 200 mL aliquots of deionized water and subsequently dispersed in 110 mL of deionized water. The final concentration of the Fe_3O_4 NP suspension was 20 mg mL^{-1}. Zeta potentials of Fe_3O_4 NPs in aqueous solutions under various conditions of pH were measured by a zeta potential analyzer (Malvern Instruments, Malvern, UK).

Fulvic acid (FA; Suwannee River 2S101F) was purchased from the International Humic Substances Society (IHSS). ^{13}C NMR estimates of carbon distribution (Table 1) and acidic functional groups and elemental compositions (Table 2) of FA are given. FA was dissolved in deionized water. The solution was kept in a shaker at room temperature (25 ± 1 °C) for 12 h to dissolve completely and then filtered through a 0.45 μm fiber membrane (MF Cat No: HAWP04700) before use. The FA stock solution was diluted to a series of concentrations ranging from 5 to 100 mg L^{-1}. The pH of each FA solution was adjusted to the desired value by adding NaOH and HCl solution. Ultrapure Milli-Q water (OHM ≥ 18.3 MΩ CM, conductivity ≤ 10 μs cm^{-1}) produced by the Milli-Q Advantage System (Millipore, USA) was used for all experiments.

Table 1 ^{13}C NMR estimates of carbon distribution of FA

Carbon distribution (ppm)							
Sample	Carbonyl 220–190	Carboxyl 190–165	Aromatic 165–110	Acetal 110–90	Hetero Aliphatic 90–60	Aliphatic 60–0	Aromatic/aliphatic
FA	5	17	22	6	16	35	0.63

Characterization of Fe_3O_4 NPs and Fe_3O_4 NPs–FA

Zeta potentials of Fe_3O_4 NPs were measured at various pHs by use of a Nano-ZS90 Zetasizer (Malvern, UK). Fe_3O_4 NPs were visualized by use of Transmission electron micrograph (TEM; H7500 Hitachi, Japan) and photographed. The TEM was operated at 120 kV. TEM images were recorded on a H7500 transmission electron micrograph (Hitachi, Japan) operated at 120 kV.

Batch adsorption experiments

All batch experiments were conducted at room temperature (25 °C ± 1 °C). The Fe_3O_4 NP suspension with concentration of 20 mg mL^{-1} was sonicated for 30 min. A total of 0.5 mL of the Fe_3O_4 NPs sonicated suspension was added to FA solution. The final volume of mixture was 50 mL. The solution pH was adjusted by adding 0.1 M HCl or NaOH. Ionic strength was controlled to 0.01 M with 1 M NaCl solution.

Adsorption isotherms were developed from data collected by adding Fe_3O_4 NPs to various initial, nominal concentrations of FA (5, 10, 20, 40, 60, 80, or 100 mg FA L^{-1}). The mixture was stirred on a rotary shaker for 24 h. The supernatant was separated from the suspension by use of a magnet then filtered through a 0.45-μm fiber membrane. The change in absorbance of the supernatant was obtained using a UV–Vis spectrophotometer operating at 254 nm. The adsorption isotherm was fitted using both Langmuir and Freundlich adsorption isotherm models. To investigate effect of pHs on adsorption, a series of suspension samples were prepared by adding Fe_3O_4 NPs into FA solution (50 mg L^{-1}), adjusting each mixture to pH 4.0, 5.0, 6.0, 7.0, 8.0, 9.0, or 10.0. The mixture was stirred for 24 h, then separated, and filtered as above. UV–Vis spectrophotometer at 254 nm was used to measure absorbance. The amount of adsorbed FA (q_e) as milligrams per gram was calculated via Eq. (1) (Hassani et al. 2015a, b):

$$q_e = \frac{(C_0 - C_e) \times V}{M} \quad (1)$$

where C_0 (mg L^{-1}) and C_e (mg L^{-1}) are the initial and equilibrium concentrations of the FA, respectively. Moreover, V (L) is the volume of the solution and M (g) is the mass of the adsorbent.

Adsorption kinetics were determined by adding 0.5 mL Fe_3O_4 NPs (20 mg mL^{-1}) suspension to the initial FA concentration of 40 mg L^{-1} measured after various durations. The pH of the suspension was adjusted to 4.0. The suspension was stirred in a shaker. A series of samples were prepared by separating the supernatant from each suspension by a magnet after 10, 15, 30, 60, 90, 120, 180, 240, and 360 min and filtered through a 0.45-μm fiber membrane. The change of each supernatant sample's absorbance was analyzed by a UV–Vis spectrophotometer (254 nm). Absorbance was used to quantify FA by comparing to an external standard curve of known concentrations of FA.

To further investigate adsorption thermodynamics, the amount of FA adsorbed by 0.5 mL Fe_3O_4 NPs (20 mg mL^{-1}) suspension at the initial FA concentration of 50 mg L^{-1} under different temperatures was measured. The pH of the aqueous suspension was adjusted to 4.0. A series of aqueous suspensions were stirred in a temperature-controlled shaker for 24 h at various temperatures of 20, 25, 30, 35, and 40 °C. The supernatant of each sample was separated by a magnet then filtered through a 0.45-μm fiber membrane. The change of adsorption kinetic in each supernatant sample was measured by UV–Vis spectrophotometer at 254 nm.

Sedimentation of Fe_3O_4 NPs and Fe_3O_4 NPs–FA

The suspension of Fe_3O_4 NPs with a concentration of 20 mg mL^{-1} was sonicated for 30 min. A total of 0.5 mL of

Table 2 Acidic functional groups and elemental compositions of FA

Sample	Acid functional groups (m mol g^{-1})			Element constitution %(w/w)					
	Carboxyl	Phenolic	Ash	C	H	O	N	S	P
FA	11.17	2.84	0.58	52.34	4.36	42.20	0.67	0.46	0.004

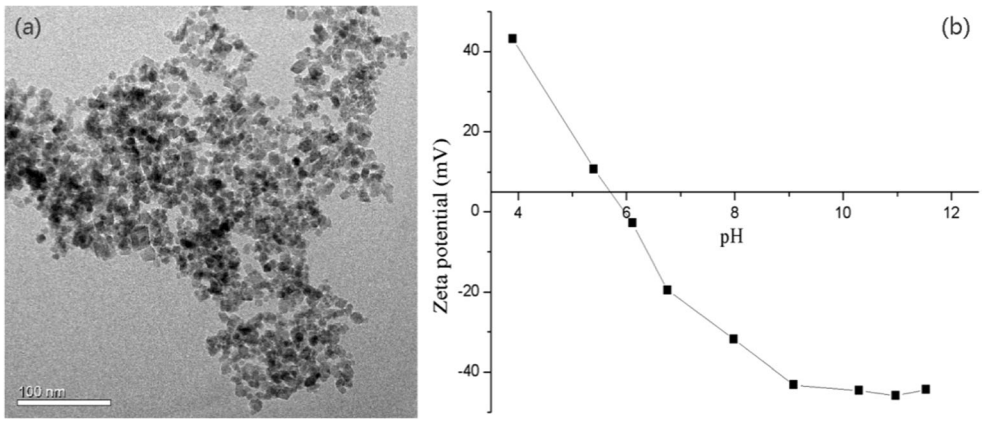

Fig. 1 TEM of Fe_3O_4 NPs (**a**) and zeta potential of Fe_3O_4 NPs in solution varying with pH (**b**)

the sonicated suspension was added into a series of 50 mL FA solutions with concentrations of 10, 20, 40, 60, and 80 mg L^{-1}. The pH of each suspension sample was adjusted to 4.0 using a 0.1-M HCl solution. The sedimentation behavior of Fe_3O_4 NPs in each suspension was evaluated by measuring the absorbance at 381 nm by use of a UV–Vis spectrophotometer. The ratio of the absorbance C_e measured at different time intervals in respect to the initial absorbance C_0 was calculated. A lesser ratio indicates that more Fe_3O_4 NPs have been accumulated and are proportional to likelihood of sedimentation.

Analytical methods of zeta potential and size

A Zetasizer Nano ZS (Malvern Instruments Ltd.) was used to determine zeta potential and hydrodynamic particle size based on the Tyndall effect. All measurements were performed at 25 °C. For time-resolved DLS measurements, 1.5 mL sample was introduced into an acrylic disposable cuvette (SARSTEDT AG & Co. Germany) for DLS measurement immediately after the samples were prepared. The scattering angle was 90°. Each size measurement lasted for 60 s. Numbers of measurement of each sample were 240. The zeta potential of Fe_3O_4 NP suspension under various pH values was performed to determine the point of zero charge (PZC).

Characterization of Fe_3O_4 NPs and Fe_3O_4 NPs/FA

FTIR spectrometry of Fe_3O_4 NPs and Fe_3O_4 NPs–FA was obtained by use of a Nicolet Magna-IR 750 FTIR spectrometer (Nicolet Magna-IR 750, Nicolet) using KBr powder as background. FTIR spectra were recorded from 400 to 4000 cm^{-1} at a resolution of 4 cm^{-1} and averaged over 200 scans. XPS was used to investigate Fe_3O_4 NPs and Fe_3O_4 NPs–FA by XPS PHI Quantera SXM spectrometer equipped with a monochromatic AlKa X-ray source (1486.6 eV, 600 W, and 15 kV). Binding energies were corrected by use of adventitious C 1s calibration peak at 284.8 eV. A charge neutralizer

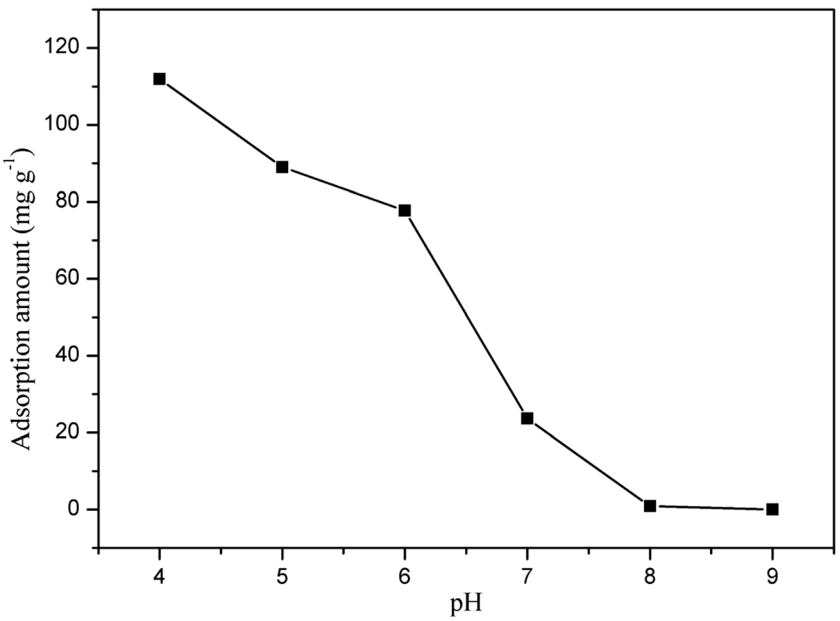

Fig. 2 Effects of pH on the adsorption of FA on Fe_3O_4 NPs

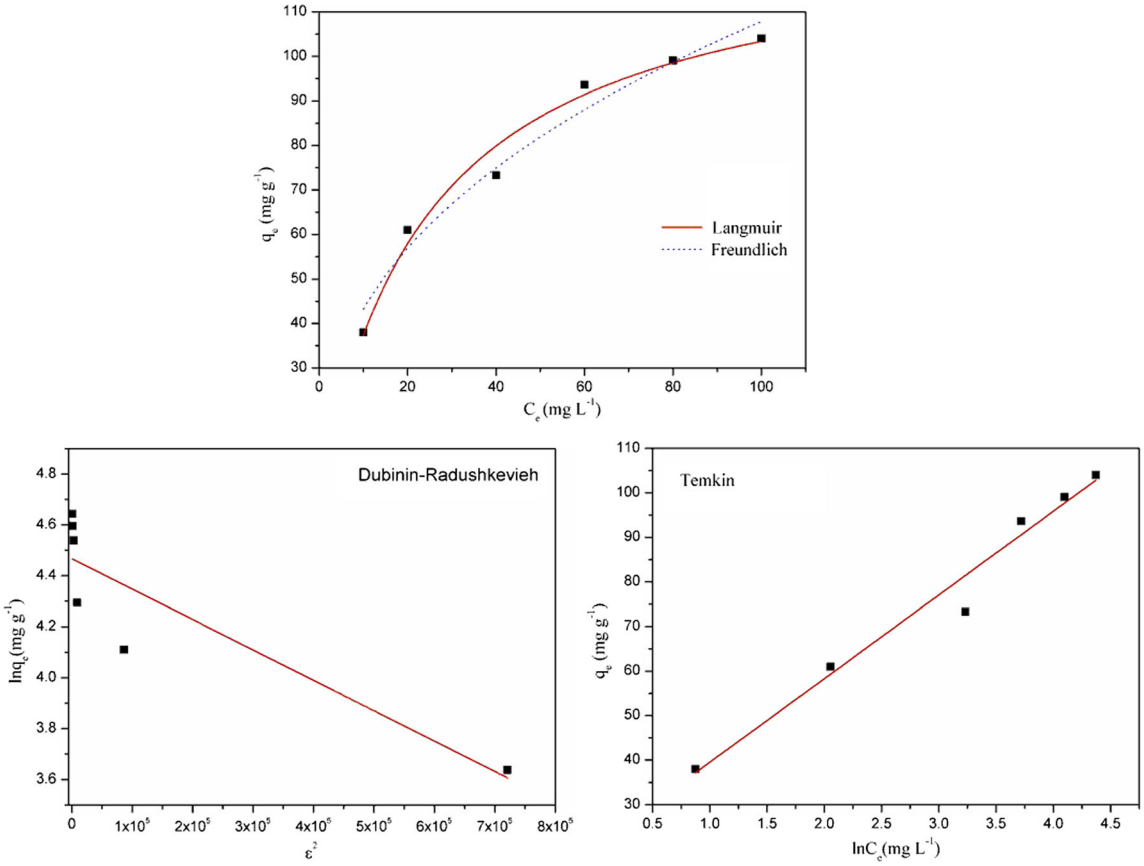

Fig. 3 Adsorption isotherm curves for adsorption of FA on the surface of Fe_3O_4 NPs; pH 4.0; dose of Fe_3O_4 NPs 10 mg; equilibrium temperature 25 °C

filament was used during all measurements to compensate for charging of the samples. High-resolution XPS was performed by use of a 0.1-eV step size and pass energy of 23.5 eV (the depth of samples analyzed ranged from 8 to 10 nm). Data processing and peak fitting were performed using XPS peak processing.

Results and discussion

Characterization of Fe_3O_4 NPs

Fe_3O_4 NPs of uniform particle size distribution were prepared by the co-precipitation method with a mean diameter of 10 nm with spherical morphology and exhibited a high degree of aggregation (Fig. 1). The isoelectric point of Fe_3O_4 NPs estimated from the measured zeta potential was 6.0.

Effects of pH

Charge density on surfaces of Fe_3O_4 will increase as the pH deviates from the isoelectric point of the NMs (Illés and Tombácz 2006). FA is negatively charged in aqueous media, so it can be adsorb on surfaces of Fe_3O_4 NPs due to electrostatic interactions. Amounts of FA adsorbed on Fe_3O_4 NPs depend on oxidation state and surface charge density of Fe_3O_4 NPs. Therefore, it is crucial to study the effect of solution pH on adsorption of FA on Fe_3O_4 NPs. Amounts of FA adsorbed on surfaces of Fe_3O_4 NPs decrease significantly with increasing pH (Fig. 2). Maximum adsorption amount of FA (112.0 mg g^{-1}) on Fe_3O_4 NPs was achieved at pH 4.0. When the solution pH > 8.0, there was no FA adsorbed on surfaces of Fe_3O_4 NPs. This is mainly because at greater pH, density of positive charges on surfaces of Fe_3O_4 NPs is less. Also, negative charges on both Fe_3O_4 NPs and FA would be more due to

Table 3 Parameters for adsorption isotherm curves for adsorption of FA on the surface of Fe_3O_4 NPs

T/K	Langmuir			Freundlich			Temkin			Dubinin–Radushkevich		
	q_m	K_L	R^2	K_F	n	R^2	α_t	b_t	R^2	q_m	$k \times 10^{-6}$	R^2
298.15	128.56	0.041	0.976	17.34	2.25	0.964	2.475	119.62	0.975	87.18	1.19	0.802

Table 4 Comparison of maximum adsorption amount of FA on various adsorbents

Material	FA sources	Adsorption amount (mg g^{-1})	pH	Size	Reference
Fe_3O_4 NPs	Suwannee River	128.6	4.0	10 nm	Present study
Mesoporous SiO_2	Nordic aquatic	22.5	3.0	50 nm	Jayalath et al. (2018)
APTES-mesoporous SiO_2	Nordic aquatic	39.5	3.0	50 nm	Jayalath et al. (2018)
SiO_2	Forest soil	77.2	4.0	100 nm	Liang et al. (2011)
Mg–Al–NO_3	Laurentian soil	153.8	9.6–10.1	n.d.	Vreysen and Maes (2008)
A raw kaolin	Bois Valor Company	14.5	3.0	n.d.	Gouré-Doubi et al. (2018)
Iron ores	lignite	2.5	7.0	12.4 μm	Zhou et al. (2016)
TiO_2^- graphene	No mention	213.0	5.0	n.d.	Zhou et al. (2014)

deprotonation carboxylic and phenolic groups (Mcdonald et al. 2004), which result in lesser electrostatic attractions. When pH was greater than the PZC of Fe_3O_4 NPs (pH = 6.0), negatively charged surfaces of Fe_3O_4 NPs would repulse negatively charged FA which would result in electrostatic repulsion and limit adsorption of FA on surfaces of Fe_3O_4 NPs. Another possible reason for this observation is that NOM was more soluble in water due to the dissociation of more hydroxyl and carboxyl functional groups at higher pH (Erhayem and Sohn 2014b). The results obtained are consistent with results of earlier studies (Kang and Xing 2008; Yang et al. 2009).

Adsorption isotherm

Isotherms for adsorption of FA on surfaces of Fe_3O_4 NPs were fitted with Langmuir (Eq. 2), Freundlich (Eq. 3), Dubinin–Radushkevich (D–R) (Eq. 4), and Temkin adsorption models (Eqs. 5 and 6) (Hassani et al. 2015a, b; Karaca et al. 2013).

$$q_e = \frac{q_m k_L C_e}{1 + k_L C_e} \tag{2}$$

$$q_e = k_F C_e^{1/n} \tag{3}$$

$$q_e = \frac{RT}{b_t} \ln a_t + \frac{RT}{b_t} \ln C_e \tag{4}$$

$$\ln q_e = \ln q_m - k\varepsilon^2 \tag{5}$$

$$\varepsilon = RT \ln\left(1 + \frac{1}{C_e}\right) \tag{6}$$

where q_e is the amount (mg g^{-1}) of adsorbed FA at equilibrium and C_e is the equilibrium FA concentration (mg L^{-1}) in solution. q_m (mg g^{-1}) represents the maximum adsorption capacity, k_L (L g^{-1}) is the Langmuir equilibrium constant, and k_F ($mg^{1-(1/n)}L^{1/n}$ g^{-1}) and n are the Freundlich parameters. k is a constant related to adsorption capacity (mg^2 mg^{-2}), and a_t and b_t are the constants of the equation. R is the gas constant (8.314 J $(mol\ K)^{-1}$), T is the thermodynamic temperature (K), and ε is the Polanyi potential.

The adsorption isotherms of FA adequately described adsorption of FA on surface Fe_3O_4 NPs (Fig. 3). The fitting results of adsorption isotherm are shown in Table 3. The order of correlation coefficient (R^2) values were $R^2L > R^2T > R^2F > R^2D$–R, which indicated that adsorption of FA on Fe_3O_4 NPs is likely a maximum, monolayer surface coverage, and adsorption site energy is a constant (Chung et al. 2015). At 25 °C and pH = 4.0, the maximum amount of FA adsorbed predicted by use of the Langmuir model was 128.6 mg g^{-1}. The maximum adsorption amount of FA on the Fe_3O_4 NPs was greater than that of other adsorbents, such as SiO_2, APTES-mesoporous SiO_2, kaolin, and iron ores, but lower than synthetic materials (Table 4) (Gouré-Doubi et al., Jayalath et al. 2018; Liang et al. 2011; Vreysen and Maes 2008; Zhou et al. 2014; Zhou et al. 2016). The constant for strength of adsorption predicted by use of the Freundlich equation was 2.52, which indicated that Fe_3O_4 NPs have a strong adsorption capacity and affinity for FA at pH 4.0. This is mainly because pH = 4.0 is less than the PZC of Fe_3O_4 NPs, which leads to more positively charged surfaces on Fe_3O_4 NPs, which, in turn, promotes adsorption of negatively charged FA via electrostatic attraction.

Adsorption kinetics

Adsorption kinetics is a key to understanding and predicting environmental behavior of Fe_3O_4 NPs in aqueous environments. At pH = 4.0, kinetics of adsorption of FA on surfaces of Fe_3O_4 NPs increased rapidly in the first 60 min; then,

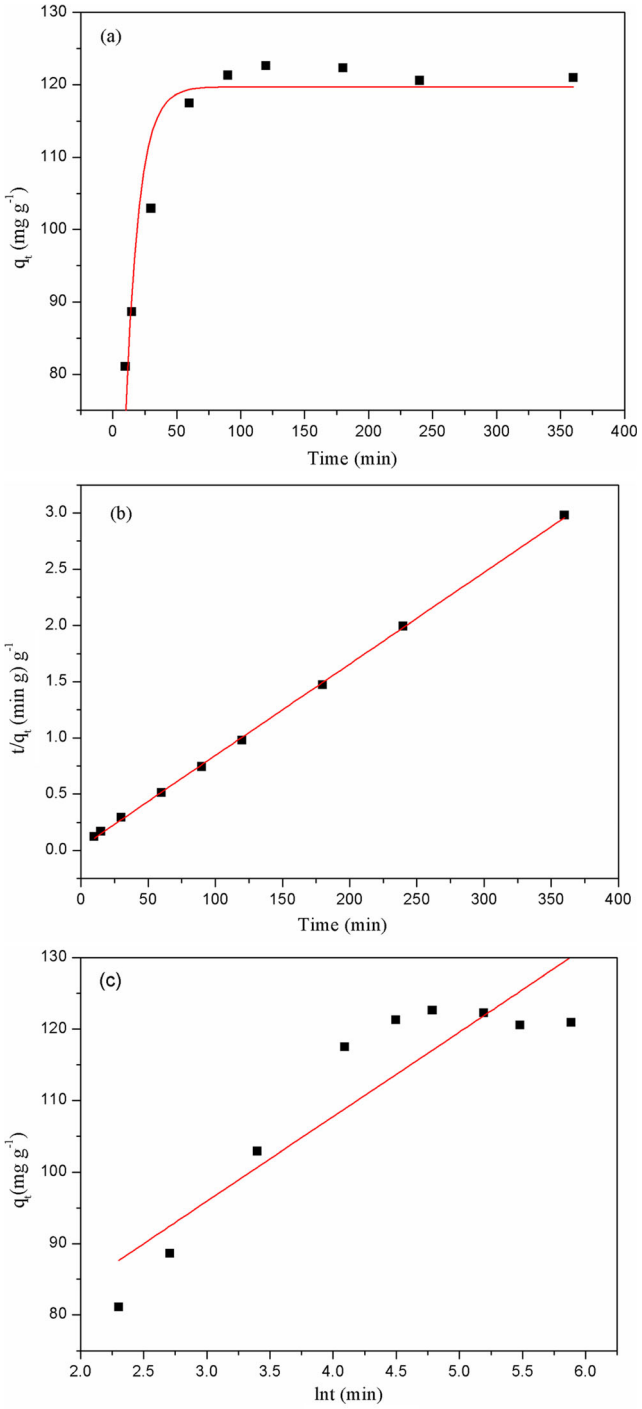

Fig. 4 Fitted pseudo-first-order (**a**), pseudo-second-order (**b**), and Elovich kinetic (**c**) for adsorption of FA on Fe_3O_4 NPs at pH 4.0

uptake of FA gradually reached steady state after about 120 min (Fig. 4a). Sizes of Fe_3O_4 NPs studied were nominally 10 nm in diameter and have a larger external surface area and reduced diffusion distance in solution than similar bulk materials. Since electrostatic attraction is the main interaction between FA and Fe_3O_4 NPs, these features enhance the rate of adsorption for the uptake of FA on Fe_3O_4 NPs. Data for kinetics of adsorption were analyzed by use of the pseudo-first-order (Eq. 7), pseudo-second-order models (Eq. 8) and Elovich models (Eq. 9) (Hassani et al. 2015a, b; Karaca et al. 2013).

$$\text{Pseudo-first-ordermodels}: q_t = q_e\left(1-e^{-k_1 t}\right) \quad (7)$$

$$\text{Pseudo-second-ordermodels}: \frac{t}{q_t} = \frac{1}{k_2 {q_e}^2} + \frac{1}{q_e}t \quad (8)$$

$$\text{Elovichmodels}: \quad q_t = A + K_t \ln t \quad (9)$$

Initial sorption rate, h_0 (mg/g/min), can be defined (Eq. 10).

$$h_0 = k_2 {q_e}^2 (t \rightarrow 0) \quad (10)$$

where k_1 (min^{-1}) and k_2 (g mg^{-1} min^{-1}) are the rate constant of adsorption for pseudo-first and second isotherms, q_t is the amount of FA at any time (mg g^{-1}), q_e is equilibrium adsorption amount of FA (mg g^{-1}), K_t is rate constant of Elovich models(mg·g^{-1}), and A is constant(mg g^{-1}·min^{-1}). The initial adsorption rate, h_0 (mg g^{-1} min^{-1}), was calculated (Table 5) and shown graphically (Fig. 4). The k_2 and h_0 were calculated from the slope and the intercept of the t/q_t to t.

Figure 4 compares adsorption kinetics of FA on surfaces Fe_3O_4 NPs. Adsorption of FA on surfaces of Fe_3O_4 NPs exhibited rate constants of constants k_1 and k_2 of 9.61×10^{-2} and 2.28×10^{-3} g mg^{-1} min^{-1}, respectively (Table 5). The initial adsorption rate h_0 was 34.4 mg g^{-1} min^{-1}. Kinetics of adsorption of FA fit the pseudo-second-order kinetic model ($R^2 = 0.999$) provide a better correlation than the pseudo-first-order kinetic model ($R^2 = 0.898$) and Elovich models ($R^2 = 0.839$). The results indicate that chemical adsorption is the rate-limiting step for FA adsorbed on Fe_3O_4 NPs; the adsorption amount of FA on the surface of Fe_3O_4 NPs is dependent on the adsorption capacity of Fe_3O_4 NPs regardless of FA concentration in solution. Adsorption amounts of FA based on the pseudo-first-order kinetic model and pseudo-second-order kinetic model were $q_e = 119.7$ and 122.9 mg g^{-1}, respectively.

Table 5 Parameters for the adsorption kinetic of FA on Fe_3O_4 NPs

	Pseudo-first-order isotherm			Pseudo-second-order isotherm				Elovich		
	k_1 (min^{-1})	q_e (mg g^{-1})	R^2	k_2 (g mg^{-1} min^{-1})	q_e (mg g^{-1})	h_0 (mg g^{-1} min^{-1})	R^2	A (mg g^{-1} min^{-1})	K_t (mg·g^{-1})	R^2
FA	0.096	119.70	0.898	2.28×10^{-3}	122.85	34.36	0.999	60.41	11.84	0.839

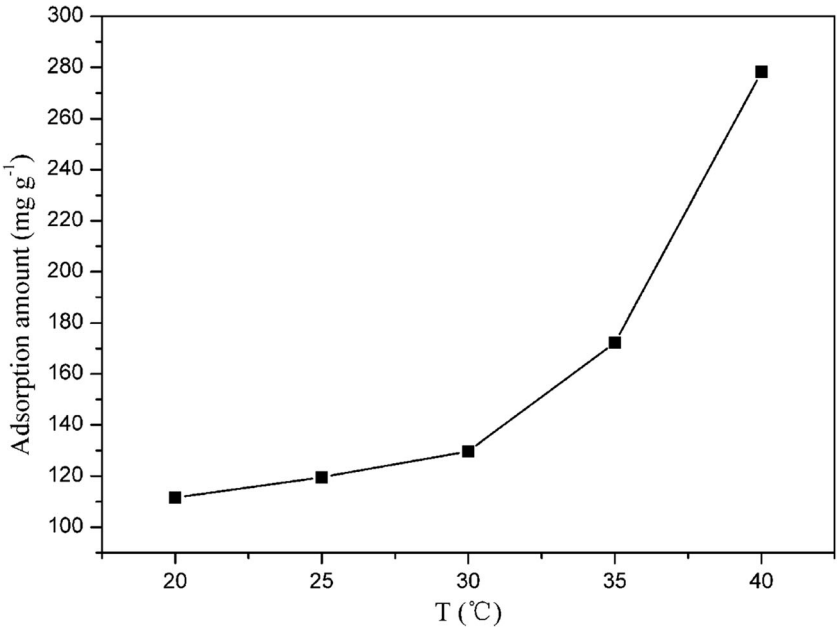

Fig. 5 Thermodynamics of FA adsorption on Fe_3O_4 NPs

Adsorption thermodynamics

Theoretically temperature affects adsorption of FA on surfaces of Fe_3O_4 NPs. When adsorption thermodynamics of FA on surfaces of Fe_3O_4 NPs was measured at various temperatures (Fig. 5), a trend of greater amounts of FA adsorbed as a function of temperature was observed. While the amount of FA adsorbed was 111.6 mg g^{-1} at 20 °C, there was only negligibly more FA adsorbed at 30 than at 20 °C, but when temperature exceeded 30 °C, amount of FA adsorbed was much greater. Furthermore, when the temperature was 40 °C, the amount of FA adsorbed was 278.3 mg g^{-1}, which is 2.8-fold greater than the amount adsorbed at 20 °C.

Thermodynamic parameters describing adsorption of FA on Fe_3O_4 NPs were obtained (Eqs. 11 and 12).

$$\log\left[\frac{q_e}{C_e}\right] = \frac{\Delta S^0}{2.303R} - \left[\frac{\Delta H^0}{2.303R}\right]\frac{1}{T} \tag{11}$$

$$\Delta G^0 = \Delta H^0 - T\Delta S^0 \tag{12}$$

where ΔG^0, ΔH^0, and ΔS^0 are the Gibbs free energy, enthalpy change, and entropy change, respectively. ΔH^0 and ΔS^0 were calculated via the slope and intercept from the $\log(q_e/C_e)$to $1/T$ curve. ΔG^0 was calculated via Eq. 6. The thermodynamic parameters for the adsorption of FA on Fe_3O_4 NPs were obtained via the thermodynamic parameters (Table 6). Thermodynamic parameters of adsorption of FA on Fe_3O_4 NPs confirmed that ΔH_0 is positive, which indicates that adsorption of FA on surfaces of Fe_3O_4 NPs is an endothermic process. The calculated ΔS_0 of Fe_3O_4 NPs is 230.5 J/mol/K, and the positive Gibbs free energy, indicating that adsorption of FA is a spontaneous process, which is in good agreement with the thermodynamic curve which showed that adsorption of FA on surfaces of Fe_3O_4 NPs is a spontaneous endothermic process, and the degree of spontaneous adsorption is directly proportional to temperature ($-\Delta G_0$ increases with the increase of temperature).

Influence of FA on the aggregation and sedimentation behavior of Fe_3O_4 NPs

In aquatic environments, fates and transformations of Fe_3O_4 NPs are strongly influenced by aggregation and sedimentation. Hydrodynamic diameters and sedimentation behavior of Fe_3O_4 NPs prior to and after adsorbed FA on its surfaces are presented (Fig. 6). In the absence of FA, there was no significant change in mean hydrodynamic diameter of Fe_3O_4 NPs with time (Fig. 6a), and sedimentation of Fe_3O_4 NPs is stabilized (Fig. 6b). This is mainly because surfaces of Fe_3O_4 NPs had significant numbers of positive charges at pH 4.0, and thus, due to electrostatic repulsion, Fe_3O_4 NPs remained at a relatively stable state and did not aggregate. There was some variation of hydrodynamic diameter and sedimentation of Fe_3O_4 NPs after FA was adsorbed on their surfaces. When

Table 6 Thermodynamic parameters for the adsorption of FA on Fe_3O_4 NPs

		$-\Delta G^0$ (KJ/mol)				
ΔH^0 (KJ/mol)	ΔS^0 (J/mol/K)	20 °C	25 °C	30 °C	35 °C	40 °C
66.03	230.51	1.509	2.661	3.814	4.967	6.119

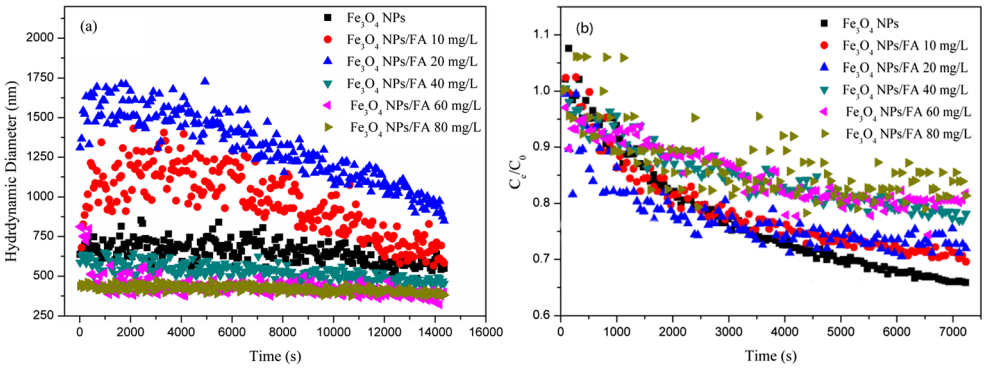

Fig. 6 Effect of amount of adsorbed FA on the hydrodynamic diameter (**a**) and sedimentation behavior (**b**) of Fe_3O_4 NPs

concentrations of FA are less than 20 mg L^{-1}, the mean hydrodynamic diameter of Fe_3O_4 NPs/FA increased gradually and suspension of Fe_3O_4 NPs/FA decreased with FA adsorbed on the surface of Fe_3O_4 NPs. This occurs when small amounts of FA are adsorbed onto surfaces of Fe_3O_4 NPs, a large portion of positive charges on surfaces of Fe_3O_4 NPs is neutralized, and surface potential is lessened which reduces electrostatic repulsion between the nanoparticles. At greater concentrations of FA, mean hydrodynamic diameter of Fe_3O_4 NPs/FA was less and substantially less of the Fe_3O_4 NPs/FA complex was observed at concentrations of FA greater than 40 mg L^{-1} and reaching a minimum at 80 mg L^{-1}. Meanwhile, suspension of Fe_3O_4 NPs/FA increased with more FA adsorbed on the surface of Fe_3O_4 NPs. This phenomenon can be explained from by two factors. With greater adsorption of FA on surfaces of Fe_3O_4 NPs, concentrations of both dissolved FA remaining in the solution and adsorbed FA would be greater; the charge repulsion would prevent the agglomeration and sedimentation of Fe_3O_4 NPs. Previous studies have also documented that adsorption and deposition of sufficient soluble organic matters on surfaces of nanosized metal oxide in aquatic systems can increase the suspendability of nanomaterials (Pettibone et al. 2008; Li et al. 2015; Kang and Xing 2008) because organic matter can cause steric hindrance and enhance the aggregation energy barrier (Guzman et al. 2006; Pelley and Tufenkji 2008). Steric hindrance of nanoparticles can be generated from organic-rich aromatic compounds and carboxylic acids present on the surface of nanoparticles (Aiken et al. 2011; Philippe et al. 2014). Therefore, FA could strongly influence the suspension/sedimentation, migration, and fate of Fe_3O_4 NPs in water environment and pose a potential impact in aquatic ecosystems.

Characterization of Fe_3O_4 NPs and Fe_3O_4 NPs/FA

Surface chemistry of adsorption was studied using FTIR, which provided information about mechanisms of adsorption. Peaks at 1206 and 1624 cm^{-1} in the spectrum of FA

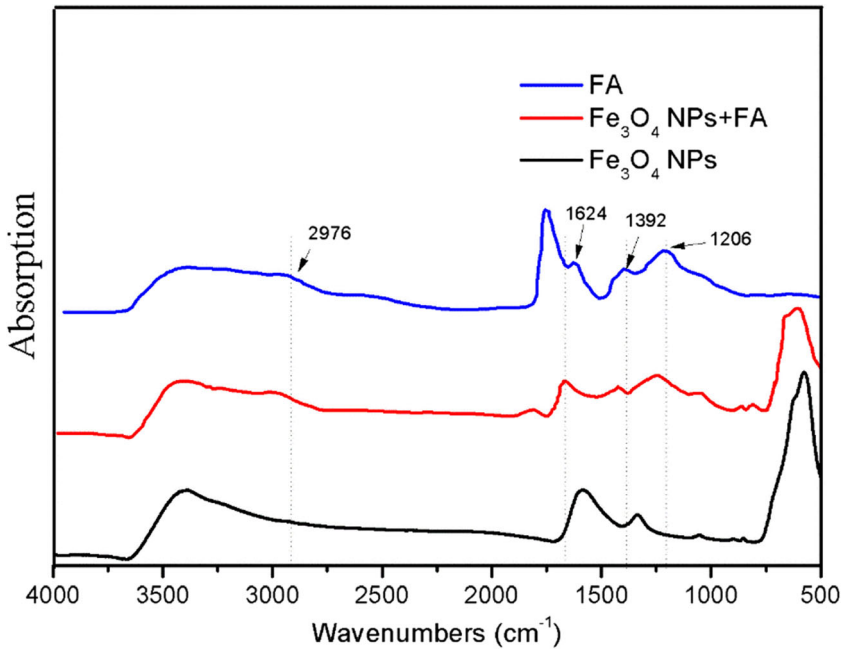

Fig. 7 FTIR of FA, Fe_3O_4 NPs, and Fe_3O_4 NPs + FA

(Fig. 7) were characteristic absorption peaks of stretching vibration of C–O in polysaccharides, skeleton vibrations of aromatic rings, or stretching vibration of the primary amide, respectively. The peak at 1392 cm^{-1} was characteristic absorption peak of deformation vibration of C–O in carboxyl groups or asymmetric stretching vibration of phenolic hydroxyl groups. Peaks at 2976 and 2940 cm^{-1} were characteristic absorption peaks of dissymmetrical and symmetrical stretching vibrations of aliphatic $–CH_2$ or $–CH_3$. In the spectrum of the Fe_3O_4 NPs/FA complex, the peak at 1206 cm^{-1} was shifted to 1250 cm^{-1}, which is indicative of adsorption of polysaccharides. Adsorption of aromatic or primary amide can be further distinguished from the shifting of the 1630 cm^{-1} band in FA to the 1680 cm^{-1} band in Fe_3O_4 NPs/FA. When compared to the spectrum of Fe_3O_4 NPs, there were significant differences in the FTIR spectrum of Fe_3O_4 NPs/FA. Peaks at 2976 and 2940 cm^{-1} were characteristic absorption peaks of stretching vibrations of $–CH_2$ or $–CH_3$ in aliphatic groups. Adsorption of C–O in carboxyl group on surfaces of Fe_3O_4 NPs is represented by shifting of the 1392 cm^{-1} bands of FA to the 1425 cm^{-1} bands of Fe_3O_4 NPs/FA. These results indicate successful adsorption of FA on surfaces of Fe_3O_4 NPs, and FA adsorbed on Fe_3O_4 NPs is mainly through ion pairing.

XPS is useful for investigating mechanisms of adsorption. XPS spectrum of FA prior to and after adsorbed on Fe_3O_4 NPs are shown in Fig. 8. Peaks of Fe 2p 1/2 and Fe 2p 2/3 also decreased in the spectrum of Fe_3O_4 NPs/FA, which indicated that FA successfully adsorbed on surfaces of Fe_3O_4 NPs. The appearance of peaks of Ni, Ce, Sn and Co might be due to impurities in Fe_3O_4 NPs. XPS spectra of Fe, C, N, and O are shown (Fig. 9). In the Fe spectrum of Fe_3O_4 NPs, the two peaks at binding energy of 724.6 and 710.9 eV represent Fe 2p 1/2 and Fe 2p 2/3, respectively. After reaction with FA, the distance between those two peaks increases compared what it was prior to adsorption, which indicated that FA adsorbed on Fe_3O_4 NPs via chemical binding. Also, intensities of those two peaks both decreases after adsorption, which can be attributed to FA adsorbed on the surface of Fe_3O_4 NPs, which could then mask peaks of Fe on the surface.

Survey scans of carbon (C1s), nitrogen (N1s), and oxide (O1s) of Fe_3O_4 NPs and Fe_3O_4 NPs/FA were conducted to identify changes prior to and after adsorption. The C1s region can be deconvoluted into three peaks at 288.7, 285.4, and 284.7 eV prior to adsorption. After FA adsorbed, a significant change was observed at binding energy of 286.3 eV, which was attributed to FA adsorbed on Fe_3O_4 NPs. The N 1s spectrum exhibited no significant change between prior to and after adsorption of FA on Fe_3O_4 NPs. The peak of nitrogen before adsorption was mainly caused by nitrogen protection during preparation of Fe_3O_4 NPs. This indicated N is not the main element involved in the adsorption of FA. The binding energy of O1s prior to adsorption can be deconvoluted into 530.1 and 531.1 eV, corresponding to the lattice O^{2-} from metallic oxides (O_{latt}) (Tang et al. 2016). After FA adsorbed on the Fe_3O_4 NPs, binding energy of O1s changes from 531.1 (O_{latt}) to 531.5 eV (O_{ad}), which means oxygen in organic acid or other organic matter formed chemical binding with Fe_3O_4 NPs. The change of O_{ad}/O_{latt} was attributed to adsorption of FA on Fe_3O_4 NPs.

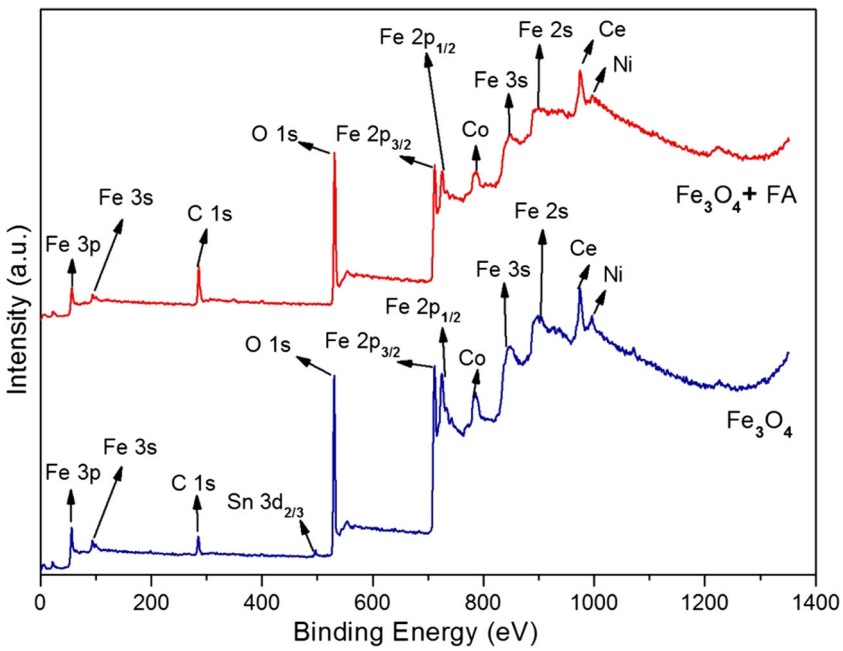

Fig. 8 XPS spectra of Fe_3O_4 NPs and Fe_3O_4 NPs + FA

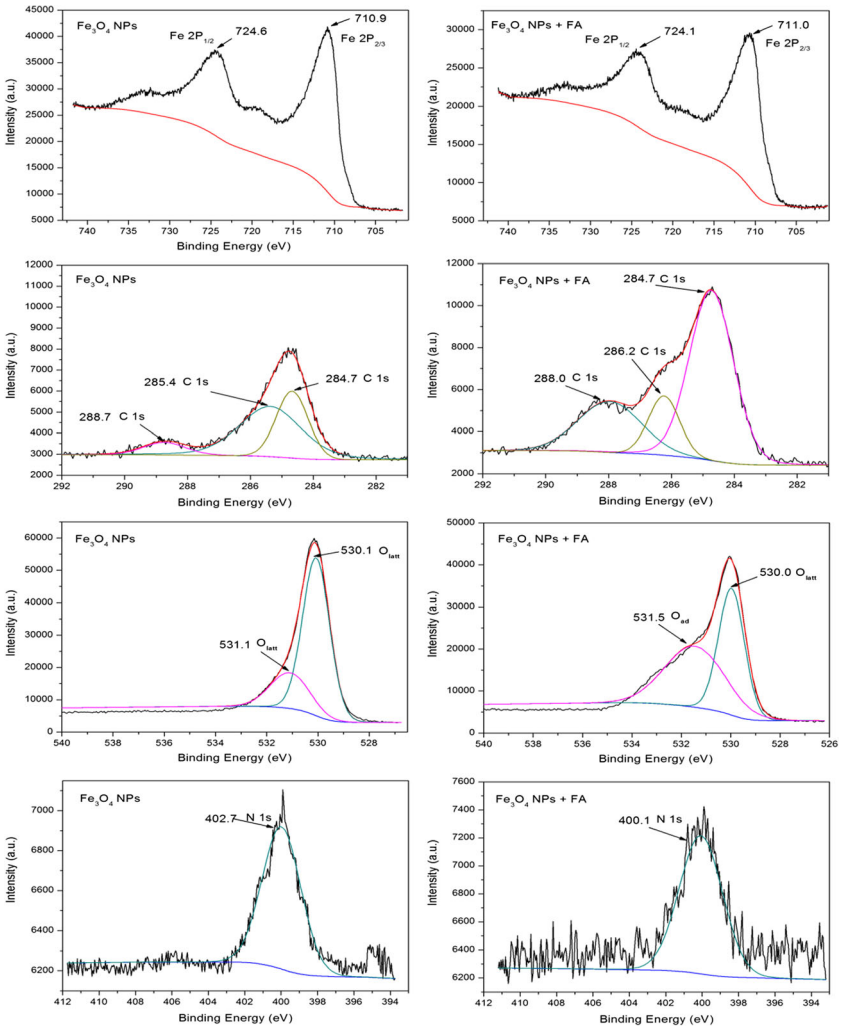

Fig. 9 XPS spectra of C1s, N1s, and O1s for Fe_3O_4 NPs and Fe_3O_4 NPs + FA

Conclusions

In the present study, solution pH was found to affect adsorption of FA on Fe_3O_4 NPs. The amount of FA adsorbed decreased with the increasing of solution pH. The adsorption isotherm of FA on Fe_3O_4 NPs was well described by both Langmuir and Freundlich models, and maximum amount of FA adsorbed was 128.6 mg L^{-1} at pH 4.0. The adsorption kinetic curve revealed a large portion of FA was adsorbed on Fe_3O_4 NPs in the first 60 min, and maximum adsorption of FA was reached within 120 min. Thermodynamic curves demonstrated that adsorption of FA on surfaces of Fe_3O_4 NPs is a spontaneous endothermic process, and at higher temperature, the endothermic process is more spontaneous. Aggregation and sedimentation of Fe_3O_4 NPs are influenced by adsorption of FA in aqueous suspensions. At lesser concentrations of FA, suspension of Fe_3O_4 NPs was less due to neutralization of charges between FA and Fe_3O_4 NPs, when a large amount of FA was adsorbed on Fe_3O_4 NPs. Electrostatic repulsion and steric hindrance would significantly increase suspension of Fe_3O_4 NPs in aqueous suspension. Results of FTIR and XPS indicated adsorption of FA on Fe_3O_4 NPs is mainly through chemical reaction, and carbohydrate carbon was important in adsorption of FA on Fe_3O_4 NPs.

Funding information This research was financially supported by the National Natural Science Foundation of China (No. 41673131).

References

Aiken GR, HsuKim H, Ryan JN (2011) Influence of dissolved organic matter on the environmental fate of metals, nanoparticles, and colloids. Environ Sci Technol. 45(8):3196–3201

Baalousha M (2009) Aggregation and disaggregation of iron oxide nanoparticles: influence of particle concentration, pH and natural organic matter. Sci Total Environ 407(6):2093–2101

Barhoumi L, Dewez D (2013) Toxicity of superparamagnetic iron oxide nanoparticles on green alga chlorella vulgaris. Biomed Res Int 2013: 647974

Chappell MA, George AJ, Dontsova KM, Porter BE, Price CL, Zhou P, Morikawa E, Kennedy AJ, Steevens JA (2009) Surfactive stabilization of multi-walled carbon nanotube dispersions with dissolved humic substances. Environ Pollut 157(4):1081–1087

Chung HK, Kim WH, Park J, Cho J, Jeong TY, Park PK (2015) Application of Langmuir and Freundlich isotherms to predict adsorbate removal efficiency or required amount of adsorbent. J Ind Eng Chem 28(25):241–246

Erhayem M, Sohn M (2014a) Effect of humic acid source on humic acid adsorption onto titanium dioxide nanoparticles. Sci Total Environ 468-469:249–257

Erhayem M, Sohn M (2014b) Effect of humic acid source on humic acid adsorption onto titanium dioxide nanoparticles. Sci Total Environ 470-471:92–98

Gouré-Doubi H, Martias C, Smith A, Villandier N, Sol V, Gloaguen V, Feuillade G (2018) Adsorption of fulvic and humic like acids on surfaces of clays: relation with SUVA index and acidity. Appl Clay Sci 154:83–90

Guzman KAD, Finnegan MP, Banfield JF (2006) Influence of surface potential on aggregation and transport of titania nanoparticles. Environ Sci Technol 40(24):7688–7693

Hassani A, Khataee A, Karaca S, Karaca M, Kıranşana M (2015a) Adsorption of two cationic textile dyes from water with modified nanoclay: a comparative study by using central composite design. J Environ Chem Eng 3(4):2738–2749

Hassani A, Khataee A, Karaca S, Shirzad-Siboni M (2015b) Surfactant-modified montmorillonite as a nanosized adsorbent for removal of an insecticide: kinetic and isotherm studies. Environ Technol 36(24):3125–3135

Hassani A, Karaca C, Karaca S, Khataee A, Açışlı Ö, Yılmaz B (2018a) Enhanced removal of basic violet 10 by heterogeneous sono-Fenton process using magnetite nanoparticles. Ultrason Sonochem 42:390–402

Hassani A, Karaca M, Karaca S, Khataee A, Açışlı Ö, Yılmaz B (2018b) Preparation of magnetite nanoparticles by high-energy planetary ball mill and its application for ciprofloxacin degradation through heterogeneous Fenton process. J Environ Manag 211:53–62

He ML, Chen YT, Yan YQ, Zhou SM, Wang CH (2017) Influence of interaction between α-Fe_2O_3 nanoparticles and dissolved fulvic acid on the physiological responses in Synechococcus sp. PCC7942. Bull Environ Contam Toxicol 99(6):719–727

Hu J, Chen GH, Lo MCI (2005) Removal and recovery of Cr (VI) from wastewater by maghemite nanoparticles. Water Res 39(18):4528–4536

Hyung H, Kim JH (2008) Natural organic matter (NOM) adsorption to multi-walled carbon nanotubes: effect of NOM characteristics and water quality parameters. Environ Sci Technol. 42(12):4416–4421

Illés E, Tombácz E (2006) The effect of humic acid adsorption on pH-dependent surface charging and aggregation of magnetite nanoparticles. J Colloid Interface Sci 295(1):115–123

Jayalath S, Larsen SC, Grassian VH (2018) Surface adsorption of Nordic aquatic fulvic acid on amine-functionalized and non-functionalized mesoporous silica nanoparticles. Environ Sci Nano 5:2162–2171

Kang SH, Xing BS (2008) Humic acid fractionation upon sequential adsorption onto goethite. Langmuir 24(6):2525–2531

Karaca S, Gürses A, Açışlı Ö, Hassani A, Kıranşan M, Yıkılmaz K (2013) Modeling of adsorption isotherms and kinetics of Remazol Red RB adsorption from aqueous solution by modified clay. Desalin Water Treat 51(13–15):2726–2739

Katsnelson BA, Degtyareva TD, Minigalieva II, Privalova LI, Kuzmin SV, Yeremenko OS, Kireyeva EP, Sutunkova MP, Valamina II, Khodos MY, Kozitsina AN, Shur VY, Vazhenin VA, Potapov AP, Morozova MV (2011) Subchronic systemic toxicity and bioaccumulation of Fe_3O_4 nano- and microparticles following repeated intraperitoneal administration to rats. Int J Toxicol 30(1):59–68

Li A, Xu MJ, Li WH, Wang XJ, Dai JY (2008) Adsorption characterizations of fulvic acid fractions onto kaolinite. J Environ Sci 20(5):528–535

Li YJ, Yang C, Guo XT, Dang Z, Li XQ, Zhang Q (2015) Effects of humic acids on the aggregation and sorption of nano-TiO_2. Chemosphere 119:171–176

Liang L, Luo L, Zhang SZ (2011) Adsorption and desorption of humic and fulvic acids on SiO2 particles at nano- and micro-scales. Colloid Surface A 384(1–3):126–130

Limbach LK, Li Y, Grass RN, Brunner TJ, Hintermann MA, Muller M, Gunther D, Stark WJ (2005) Oxide nanoparticle uptake in human lung fibroblasts: effects of particle size, agglomeration, and diffusion at low concentrations. Environ. Sci. Technol. 39(23):9370–9376

Lin DH, Liu N, Yang K, Zhu LZ, Xu Y, Xing BS (2009) The effect of ionic strength and pH on the stability of tannic acid-facilitated carbon nanotube suspensions. Carbon 47(12):2875–2882

Mashjoor S, Yousefzadi M, Zolgharnain H, Kamrani E, Alishahi M (2018) Organic and inorganic nano-Fe_3O_4: alga ulva flexuosa-based synthesis, antimicrobial effects and acute toxicity to briny water rotifer *Brachionus rotundiformis*. Environ Pollut 237:50–64

Mcdonald S, Bishop AG, Prenzler PD, Robards K (2004) Analytical chemistry of freshwater humic substances. Anal Chim Acta 527(2):105–124

Pan B, Xing BS (2008) Adsorption mechanisms of organic chemicals on carbon nanotubes. Environ Sci Technol 42(24):9005–9013

Panessa-Warren BJ, Maye MM, Warren JB, Crosson KM (2009) Single walled carbon nanotube reactivity and cytotoxicity following extended aqueous exposure. Environ Pollut 157(4):1140–1151

Parfitt RL, Fraser AR, Farmer VC (2006) Adsorption on hydrous oxides. III. Fulvic acid and humic acid on goethite, gibbsite and imogolite. Eur J Soil Sci 28(2):289–296

Philippe A, Schaumann GE (2014) Interactions of dissolved organic matter with natural and engineered inorganic colloids: A Review. Environ Sci Technol. 48(16):8946–8962.

Pelley AJ, Tufenkji N (2008) Effect of particle size and natural organic matter on the migration of nano- and microscale latex particles in saturated porous media. J Colloid Interface Sci 321(1):74–83

Pettibone JM, Cwiertny DM, Scherer M, Grassian VH (2008) Adsorption of organic acids on TiO_2 nanoparticles: effects of pH, nanoparticle size, and nanoparticle aggregation. Langmuir 24(13):6659–6667

Tang Z, Zhao XL, Zhao TH, Wang H, Wang PF, Wu FC et al (2016) Magnetic nanoparticles interaction with humic acid: in the presence of surfactants. Environ Sci Technol 50(16):8640–8648

Vreysen S, Maes A (2008) Adsorption mechanism of humic and fulvic acid onto Mg/Al layered double hydroxides. Appl Clay Sci 38:237–249

Wei SY, Xiang WJ (2013) Adsorption removal of Pb(II) from aqueous solution by fulvic acid-coated ferrihydrite. J Food Agric Environ 11(2):1376–1380

Weng L, Van Riemsdijk WH, Koopal LK, Hiemstra T (2006) Adsorption of humic substances on goethite: comparison between humic acids and fulvic acids. Environ Sci Technol 40(24):7494–7500

Yang K, Lin DH, Xing BS (2009) Interactions of humic acid with nanosized inorganic oxides. Langmuir 25(6):3571–3576

Zhou Q, Zhong YH, Chen X, Liu JH, Huang XJ, Wu YC (2014) Adsorption and photocatalysis removal of fulvic acid by TiO2–graphene composites. J Mater Sci 49(3):1066–1075

Zhou YL, Zhang YB, Li GH, Jiang T (2016) Effects of metal cations on the fulvic acid (FA) adsorption onto natural iron oxide in iron ore pelletizing process. Powder Technol 302:90–99